Proc. Natl. Acad. Sci. USA
Vol. 89, pp. 2499–2503, March 1992
Biophysics

Structure of the histidine-containing phosphocarrier protein HPr from *Bacillus subtilis* at 2.0-Å resolution

OSNAT HERZBERG*†, PRASAD REDDY‡, SARAH SUTRINA§, MILTON H. SAIER, JR.§, JONATHAN REIZER§, AND GEETA KAPADIA*

*Maryland Biotechnology Institute, University of Maryland, and ‡National Institute of Standards and Technology, Center for Advanced Research in Biotechnology, 9600 Gudelsky Drive, Rockville, MD 20850; and §Department of Biology, University of California, San Diego, La Jolla, CA 92093-0116

Communicated by David R. Davies, December 3, 1991 (received for review September 30, 1991)

ABSTRACT **The crystal structure of the histidine-containing phosphocarrier protein (HPr) of the phospho*enol*pyruvate:sugar phosphotransferase system (PTS) from *Bacillus subtilis* has been determined at 2.0-Å resolution and refined to a crystallographic residual error *R*-factor of 0.150. The secondary-structure folding topology of the molecule is that of an open-face β-sandwich formed by four antiparallel β-strands packed against three α-helices. The active-site histidine, His-15, caps the N terminus of the first helix, suggesting that the helix dipole plays a role in stabilizing the phosphorylated state of the histidine. A sulfate anion located between His-15 and the neighboring Arg-17 has been identified in the electron-density map. Association of this negatively charged species with the two key catalytic residues implies that the crystal structure resembles the phosphorylated state of the protein. A model of the phosphorylated form of the molecule is proposed, in which the negatively charged phosphoryl group interacts with two main-chain nitrogen atoms of the following helix and with the guanidinium group of Arg-17. It is also proposed that the phosphoryl transfer from HPr to the IIA domain of the glucose permease involves Arg-17 switching between two salt bridges: one with the phosphorylated histidyl of HPr and the other with two aspartyl residues associated with the active site of the IIA domain of glucose permease, which are accessible upon complex formation.**

The bacterial phospho*enol*pyruvate:sugar phosphotransferase system (PTS) first described by Kundig *et al.* (1) transports some carbohydrates into the cell and simultaneously phosphorylates them to initiate their metabolism and prevent leakage from the cytoplasm. This system also plays a role in chemotaxis toward PTS sugars and in regulation of the uptake of several non-PTS sugars (for reviews, see refs. 2–5). The system consists of two general energy-coupling components [enzyme I and a histidine-containing phosphocarrier protein (HPr)] and of sugar-specific permeases (enzymes II). An enzyme II typically consists of three domains, IIA (also designated enzyme III or factor III), IIB, and IIC (6). A total of five phosphoryl group transfers occurs along the pathway: phospho*enol*pyruvate (PEP) → enzyme I → HPr → IIA → IIB → sugar. The IIC domain forms the transmembrane channel for the specific sugar.

HPr is a small protein (9 kDa), which is phosphorylated on the N^{δ} atom of a histidine residue, His-15 (7). In contrast to HPrs from Gram-negative bacteria, HPrs from Gram-positive bacteria are also phosphorylated on Ser-46 by an ATP-dependent protein kinase. This phosphoryl group is hydrolyzed by a HPr(Ser~*P*) phosphatase. It has been recently shown for the *Bacillus subtilis* system that the phosphoryl transfer from enzyme I to HPr is inhibited ≈100-fold by the serine phosphorylation (8). HPr(Ser~*P*) in Gram-positive bacteria may play a regulatory role in sugar transport, although the nature of this regulation is not clear (for review, see ref. 9).

The folding topology of HPr from *Escherichia coli* has been determined by NMR methods (10). This topology differs drastically from the topology reported for the x-ray crystal structure (11). Recently, binding of site-directed mutants of HPr to monoclonal antibodies has shown that the NMR model is consistent with a continuous surface-binding site. In contrast, the x-ray model implies discontinuous surface and, thus, is probably not correct (12). The topology of the homologous HPr from *B. subtilis* (34% identity) has been shown by NMR to resemble that of *E. coli* HPr (13, 14). The ^{1}H-NMR spectrum of the *B. subtilis* protein was found to be sensitive to phosphorylation of Ser-46. The observed backbone chemical-shift perturbations extend far away from position 46, which the authors interpreted as an indication of extensive structural changes beyond the mere addition of a negative charge. Moreover, the mutant S46D, in which Ser-46 is substituted by an aspartyl residue, had a similar spectrum to HPr(Ser-*P*), suggesting a similar conformation for both.

We present here the x-ray crystal structure determination of HPr from *B. subtilis* at 2.0-Å resolution.¶

EXPERIMENTAL METHODS

Protein Purification and Crystallization. The *B. subtilis* HPr was cloned, overproduced, and purified as described (15). Initial crystallographic work was done with the inactive mutant H15A (16). For the heavy-atom derivative work, several cysteine mutants were prepared by site-directed mutagenesis, all of which contained the catalytic His-15. Only one of these mutants (S83C) formed crystals suitable for x-ray work. The S83C HPr is active in the PTS and, therefore, further crystallographic work has been done with this mutant. The crystallization conditions are somewhat different from those used to obtain the mutant H15A HPr crystals. The vapor-diffusion method was used, but the protein/salt solution was equilibrated against reservoirs containing 68–74% saturated ammonium sulfate solution, 0.5% (wt/vol) polyethylene glycol 1000, and 100 mM citrate buffer at pH 6.2–6.4. The pH of the crystals is close to physiological pH and substantially above the pK_a of the active-site histidyl residue (17). The crystals diffract to at least 2.0-Å resolution. As the H15A mutant crystals, they belong to space group $P3_121$ (resolved from $P3_221$ by using the anomalous data of the heavy-atom derivatives) with unit cell dimensions of $a = b = 47.3$ Å; $c = 61.8$ Å; $\alpha = \beta = 90°$; $\gamma = 120°$Å.

Structure Determination. The structure was determined by using the multiple isomorphous replacement (MIR) method.

The publication costs of this article were defrayed in part by page charge payment. This article must therefore be hereby marked "*advertisement*" in accordance with 18 U.S.C. §1734 solely to indicate this fact.

Abbreviations: PTS, phospho*enol*pyruvate:sugar phosphotransferase system; HPr, histidine-containing phosphocarrier protein.

†To whom reprint requests should be addressed.

¶The atomic coordinates have been deposited in the Protein Data Bank, Chemistry Department, Brookhaven National Laboratory, Upton NY 11973 (reference, 1HPR).

Table 1. Heavy-atom derivative statistics

Compound*	Soaking time, days	R_{iso}† (2.8 Å)	Unique reflections, no.	Sites, no.	R_{cen}†	$\langle f_H \rangle / \langle E_H \rangle$†
Uranyl acetate (2 mM)	4	0.188	2150	2	0.51	1.92
$KAu(CN)_2$ (1 mM)	6	0.164	2185	1	0.52	1.77

*For soaking experiments the citrate buffer was replaced by Tris acetate.
†$R_{iso} = \Sigma_h \| F_{PH}obs| - |F_P obs| \| / \Sigma_h |F_P obs|$.
$R_{cen} = \Sigma_{h\ centric} \| F_{PH}obs| - |F_P obs + F_H calc| \| / \Sigma_{h\ centric} \| F_{PH}obs| - |F_P obs| \|$, where h, Miller indices; obs, observed; calc, calculated; F_P, F_{PH}, and F_H, native, derivative, and heavy-atom structure factors, respectively. $\langle E_H \rangle$, rms lack of closure error; $\langle f_H \rangle$, rms heavy-atom scattering.

X-ray intensity data were collected on a Siemens area detector mounted on a Siemens 3-axis goniostat. Graphite monochromated CuK_α x-rays were generated with a Rigaku Rotaflex RU-200BH rotating-anode source. The data were processed with the computer program suite XENGEN (18). Data to 2.0-Å resolution were obtained for the S83C protein. The 5083 reflection set is 90% complete, with the shell in the 2.1- to 2.0-Å range only 58% complete. The agreement between symmetry-related reflections (R_{sym}) is 0.086. Data at 2.8-Å resolution for two heavy-atom derivatives were also collected. The R_{sym} values for the uranyl and gold derivative are 0.057 and 0.070, respectively (Bijvoet-related reflections were not merged).

The multiple isomorphic replacement and solvent-flattening work was done by using the computer program suite PHASES.‖ Heavy-atom binding sites were determined from difference Patterson and difference Fourier maps in the usual manner (19). The positional parameters and occupancies of the heavy atoms were refined by lack of closure error minimization (20). Some statistics for the heavy-atom derivatives are given in Table 1. Although the protein contains an engineered cysteine residue, no mercurial derivative was obtained (the current electron-density map shows that Cys-83 is oxidized). A phase set was obtained with a mean figure of merit of 0.66. A 2.8-Å resolution electron-density map was computed with centroid phases (21) and measured structure-factor amplitudes weighted by the figure of merit. The map showed continuous stretches of density that were interpretable with some effort. Although the volume occupied by solvent in these crystals is rather low (44%), solvent flattening (22) proved useful in improving the map. The procedure was done as implemented in PHASES. The solvent content was specified for masking purposes as only 35%. The average cumulative phase shift from the initial MIR phases was 34°. The solvent-flattened electron-density map was easier to interpret and enabled unambiguous tracing of the polypeptide chain consistent with the known amino acid sequence. Fig. 1 shows a region of the map around the active-site histidyl residue.

A molecular model was fitted to the electron-density map on an Evans and Sutherland (Salt Lake City) PS390 interactive graphics system using the program FRODO (23). This initial model consisted of all but the first amino acid residue because the expressed protein lacks the N-terminal methionine (14).

Structure Refinement. The first stage of structure refinement was done with the program X-PLOR (24) by using the simulated annealing slow-cooling protocol at 3000 K and including data between 6.0 and 2.0 Å for which structure factor $F \geq 2\sigma(F)$. The residual error factor R was reduced from 0.441 to 0.219 ($R = \Sigma_h \| F_o| - |F_c| \| / \Sigma_h |F_o|$, where $|F_o|$ and $|F_c|$ are the observed and calculated structure factor amplitudes, respectively). After one cycle of X-PLOR refinement, interactive model building was resumed, displaying two types of electron-density maps: (*i*) a map computed with the coefficients $2|F_o| - |F_c|$ and calculated phases; (*ii*) a map computed with the coefficients $|F_o| - |F_c|$ and calculated phases. Adjustments were made to the model, and density consistent with a bound sulfate anion was identified and modeled.

For the next stage of refinement the restrained-parameter least-squares program of Hendrickson and Konnert (25), which includes a fast Fourier transform calculation (26), was used. Forty-one cycles of refinement were done with three manual refitting and the addition of 100 solvent molecules to the model.

The current model of HPr has an R-factor of 0.150 for the 4496 reflections between 8.0- and 2.0-Å resolution for which $F \geq 2\sigma(F)$ (88% of all measured data). The stereochemical parameters are well within the range known from crystal structures of small peptides: the rms distance deviations from ideal values for bond length is 0.023 Å and for bond angle is 0.043 Å.

RESULTS AND DISCUSSION

Molecular Conformation of HPr. HPr forms a classical open-face β-sandwich (27), made of a curved β-sheet consisting of four antiparallel β-strands and three helices that pack against one face of the sheet (Fig. 2). This topology is consistent with the topology of the two NMR structures (10, 14) and is in contrast to the reported topology of the *E. coli* HPr crystal structure (11), which does not form an open-face β-sandwich. The second helix seen in the current *B. subtilis* x-ray structure has not been yet identified by the NMR work on *B. subtilis* (14), but it has been identified in the *E. coli* HPr (10).

The following residues form α-helices according to the criteria of Kabsch and Sander (29): 16–26; 47–51; and 70–84. Residues in β-strands are as follows: 4–8; 32–37; 40–43; and 60–66. Each of the residues His-15 and Ser-46 forms a helix N-cap (30), such that their carbonyl oxygen atoms make the respective first *i*, *i*+4 helical hydrogen bond.

Environment of the Active Histidine. The histidyl residue with the phosphoryl transfer function, His-15, is located on the surface of the protein at the N terminus of the first α-helix (Fig. 3*a*). Its side chain caps the side of the helix cross section, stacking roughly perpendicular to the ring of Pro-18, a conserved residue in all known HPr sequences. Presumably, the invariant proline is required to minimize the electrostatic interaction between the main-chain amide hydrogen and the imidazole ring. On the other hand, the dipole of the helix N terminus may stabilize the negatively charged phosphorylated histidine.

A key interaction in the crystal is that of the sulfate anion with the guanidinium group of Arg-17 (Fig. 1), which is a conserved residue in all HPr sequences. The sulfate lies between His-15 and Arg-17, forming a salt bridge with Arg-17 side chain (2.4 Å). The sulfate also makes crystal contacts with two neighboring protein molecules. With one molecule, the sulfate forms a salt bridge with the positively charged N terminus (2.8 Å), as well as interacts with the nitrogen atom of Ile-47, and the O^γ atom of Ser-66. For the second molecule, contacts are with the nitrogen of Met-48 and the O^γ atom of Ser-46. We propose that this crystal packing facilitates the trapping of the arginine side chain in a conformation that resembles the phosphorylated state of HPr. Without the

‖Furey, W. & Swaminathan, S., 14th American Crystallographic Association Meeting, April 8–13, 1990, New Orleans, abstr. PA33.

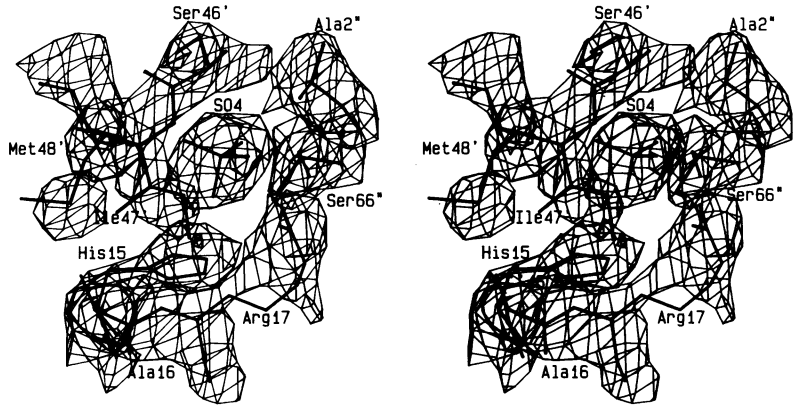

FIG. 1. Stereoscopic view of a region of the electron-density map in vicinity of the active-site His-15. The 2.8-Å solvent-flattened multiple isomorphous replacement map is displayed together with the refined model at 2.0 Å. The electron density for the sulfate anion (labeled SO4) can be seen already in this map, although it was added to the model only at advanced stage of refinement. Residues from neighboring molecules are also shown. (') is added to the labels of residues from one molecule (symmetry operator $Y, X, -Z + 1$), and (") is added to those of a second molecule (symmetry operator $X - Y + 1, -Y + 1, -Z + 2/3$).

sulfate, the electrostatic interaction of Arg-17 with the main-chain nitrogens at the N terminus of the α-helix would be repulsive.

Lack of a salt bridge interaction between His-15 and the sulfate ion (the shortest distance is 3.9 Å) suggests that the histidine is uncharged, consistent with its role as a nucleophile in the phosphoryl transfer. Although discriminating between nitrogen and carbon atoms at the resolution of the structure determination is impossible, the imidazole-ring orientation was chosen such that the N^{δ} atom, the target of phosphorylation, points toward Arg-17 and the sulfate. A hydrogen bond is formed between the Ser-12 O^{γ} atom and the N^{ϵ} atom. The close proximity of the N^{δ} atom to the two main-chain nitrogen atoms of the proceeding helix is consistent with it being deprotonated, as required for a phosphoryl acceptor.

Three hydrophobic side chains on the surface of the protein are located close to the active site: Ile-47, Met-48, and Met-51. This hydrophobic patch may indicate the site of interaction with other proteins of the PTS. Interestingly, this patch is flanked by His-15 from one side and by Ser-46 from the other side (see below).

Environment of Ser-46. Ser-46, the target of phosphorylation by the ATP-dependent HPr kinase in Gram-positive bacteria, is located on the surface at the N terminus of the second α-helix (Fig. 4). Its side chain caps the helix such that the O^{γ} atom interacts with the main-chain nitrogen atom of Gly-49 (2.9 Å). Capping of N termini of helices by serine residues is common in protein structures (30, 31). Asparagines and aspartic acids also occupy this position with a higher frequency than expected. Hydrogen bonding of the side-chain oxygen atom with the main-chain nitrogen atom is associated with this preference. Presumably, the negative charge of a phosphorylated serine can be stabilized by the helix dipole as well. However, modeling shows that when phosphorylated, the χ_1 dihedral angle of Ser-46 should be rotated by $\approx 60°$ to avoid short contacts of the phosphoryl group with the helix.

It is an interesting coincidence that the crystal packing brings the active site of one molecule and Ser-46 of a second one close to the sulfate anion. This proximity probably has no physiological significance because no evidence is available for dimer formation.

It has been recently shown that the interaction of the *B. subtilis* HPr with enzyme I is impaired by phosphorylation of Ser-46 (8). The crystal structure shows that phosphorylation of Ser-46 does not require a major rearrangement of the polypeptide chain, but the charge distribution is obviously altered. The hydrophobic patch formed by Ile-47, Met-48, and Met-51 is flanked by Ser-46 on one side and by the active site on the other and may be the region of interaction of HPr with enzyme I (and perhaps with the IIA domains of the PTS permeases). The introduction of a negative charge on Ser-46~*P* in the interface formed by the two interacting proteins could interfere with the protein–protein complex formation because of unfavorable electrostatic interactions. Similarly, when His-15 is phosphorylated, the interaction with the kinase may be prevented if the active site forms part of the interface.

Why are HPrs from Gram-positive bacteria phosphorylated on Ser-46, whereas those from Gram-negative bacteria are not? There are three residues in the vicinity of Ser-46 that are invariant in the known sequences of HPrs from Gram-

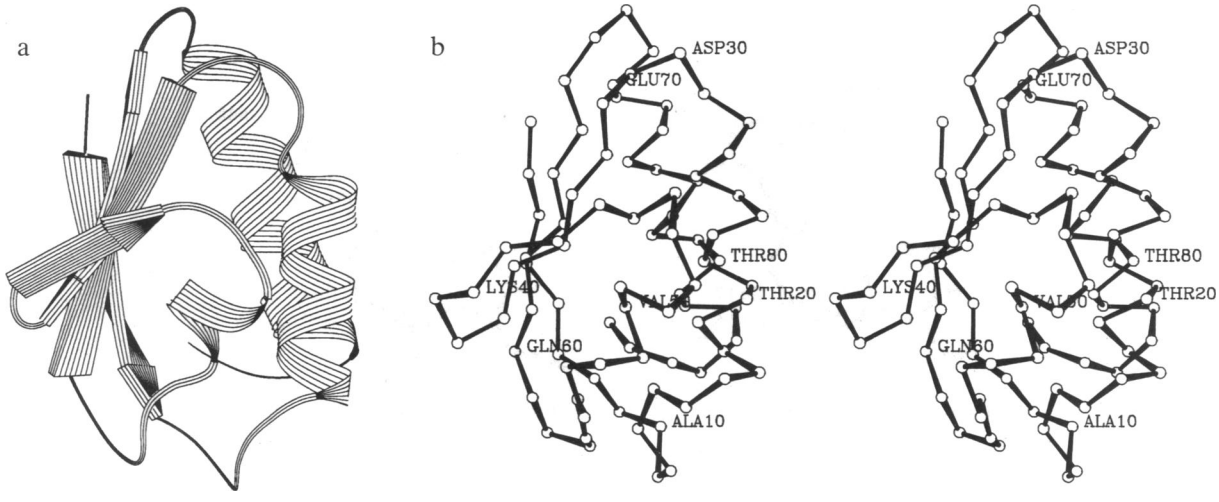

FIG. 2. Fold of HPr from *B. subtilis*. (*a*) Highlighting secondary-structure motifs. Figure was generated with the computer program RIBBON (28). (*b*) Stereoscopic representation showing α-carbon positions in the molecule. Every tenth amino acid is labeled.

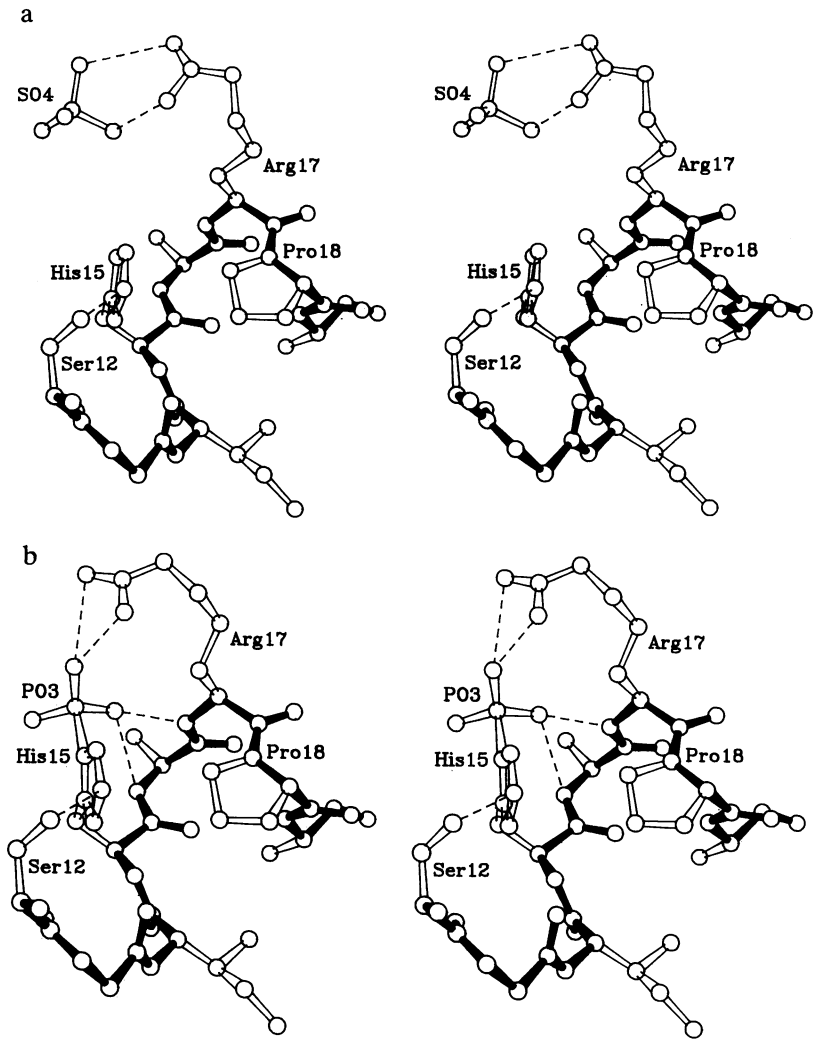

FIG. 3. Stereoscopic view of the active-site region of HPr. (*a*) Crystal structure. (*b*) Model of phosphorylated state. Bonds between main-chain atoms are filled, and those between side-chain atoms are open. Important interactions of side chains of His-15 and Arg-17 are shown by broken lines. The sulfate is labeled SO4, and the phosphate is labeled PO3.

positive bacteria but differ in the protein from *E. coli* (4): Asn-43 is a serine in *E. coli* HPr, Met-48 is a phenylalanine, and Gly-49 is a lysine. Inspection of the crystal structure (Fig. 4) shows that the last two replacements would crowd the environment of Ser-46, change the charge distribution, and potentially prevent interaction with the kinase.

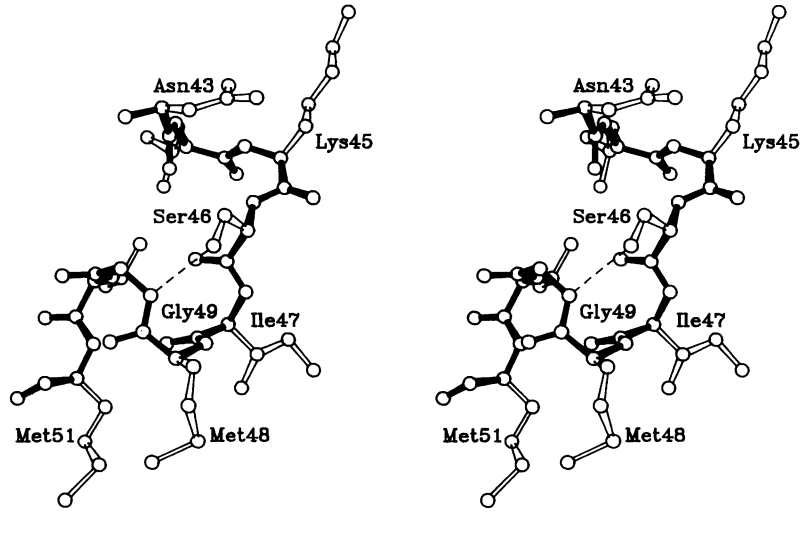

FIG. 4. Stereoscopic view of environment of Ser-46. Bonds between main-chain atoms are filled, and bonds between side-chain atoms are open. Hydrogen bond between the O^{γ} atom of Ser-46 and the main-chain nitrogen atom of Gly-49 is shown by broken line.

Model of Phosphorylated His-15. In analogy to our modeling of the phosphorylated state of the IIA domain of the glucose permease (32), a model for the activated phosphohistidine of HPr has been derived. The phosphoryl group was built so that the phosphorus atom is in the plane of the imidazole ring of His-15 (Fig. 3*b*). In contrast to the IIA domain, where no adjustments to the protein were required, minor adjustments have been made here: the χ_2 dihedral angle of His-15 was rotated by 10° to avoid short contact with the main-chain nitrogen atom of Arg-17. This rotation facilitates electrostatic interactions of the phosphoryl oxygen atom with the two main-chain nitrogens of Ala-16 and Arg-17. In addition, the χ_1 dihedral angle of Arg-17 was rotated by 40°, such that a salt bridge was formed with the phosphoryl moiety rather than with the sulfate ion, as observed in the crystal structure (Fig. 3*a*).

We propose that without a negative charge in the active site, the side-chain conformation of Arg-17 is altered to avoid the unfavorable electrostatic interaction with the dipole of the helix N terminus. In contrast, the NMR work suggests that the side chains of His-15 and Arg-17 interact also in the phosphate-free state (10, 14), implying that Arg-17 does interact with the helix N terminus. Perhaps this observation was made because the two residues are close in sequence, such that the C^{β} atom of Arg-17 is 4.2 Å apart from the side chain of His-15. However, this short distance does not imply that an electrostatic interaction should exist between the two side chains. Modeling shows that an alternative position of the guanidinium group may be obtained simply by changing the side-chain torsion angles, without invoking a major main-chain conformational transition. For example, a fully extended side-chain conformation would be acceptable. Klevit and Waygood (10) observed an interaction between Arg-17 and the C terminus of *E. coli* HPr (with either the side-chain or the backbone carboxyl group of Glu-85). An equivalent interaction has not been reported in the NMR work on the *B. subtilis* protein (14). The C terminus of the *B. subtilis* HPr (Glu-88) is remote from the active site, and the only negatively charged residue that could play such a role is Glu-84 on the C terminus of the third helix. Modeling shows that a salt bridge can be formed by modifying the dihedral angles of Arg-17 such that its side chain points away from His-15. However, there is no evidence yet that this salt bridge is essential for maintaining the structural integrity of the phosphate-free form. Any other allowed conformation of the Arg-17 side chain in which the charge is solvated and the interaction with the dipole of the helix N terminus is avoided would be equally possible.

Proposed Mechanism for Phosphoryl Transfer. The structure of HPr, in which the active-site histidine is on the protein surface, is consistent with the previously proposed mechanism of the PTS phosphoryl transfer involving the associative pathway (ref. 33; for review of phosphoryl transfer pathways, see ref. 34), and with the crystal structure of the IIA domain of the *B. subtilis* glucose permease (32). The associative pathway is required to avoid atomic clashes at the protein–protein interface. A pentacoordinated intermediate or transition state is implied, with trigonal bipyramidal geometry at the phosphorus. With the two active-site histidine nitrogen atoms (N^{δ} of His-15 in HPr and N^{ε} of His-83 in the IIA domain of glucose permease) occupying apical positions, the transfer would lead to inversion of configuration at the phosphorus.

The electrostatic interactions should be delicately balanced to permit burial of the negatively charged phosphoryl group at the protein–protein interface. We have identified two aspartate residues in the IIA domain of the glucose permease (Asp-31 and Asp-87) associated with the active site and oriented toward each other (32). Whereas the phosphohistidine of HPr is stabilized by the salt bridge with Arg-17, we propose that the transfer to the IIA domain of glucose permease is facilitated by a switch to another salt bridge in which Arg-17 interacts with the two aspartates of this IIA domain. The stability of HPr(His~*P*) is thus reduced, allowing the phosphoryl transfer to His-83 of the IIA domain of glucose permease.

We thank John Moult, Walt Stevens, Gary Gilliland, Der-Ing Liao, and Tom Poulos for many helpful discussions. Computing time for the X-PLOR refinement was provided by the National Institute of Standards and Technology (NIST). Certain commercial equipment, instruments, and materials are identified in this paper. Such identification does not imply a recommendation or endorsement by NIST. This work was supported by National Science Foundation Grant DMB-9019340 to O.H. Protein preparation was supported by National Institutes of Health Grants RO1-AI21702 and RO1-AI14176 to M.H.S.

1. Kundig, W., Ghosh, S. & Roseman, S. (1964) *Proc. Natl. Acad. Sci. USA* **52**, 1067–1074.
2. Postma, P. W. & Lengeler, J. W. (1985) *Microbiol. Rev.* **49**, 232–269.
3. Saier, M. H., Jr. (1985) *Mechanisms and Regulation of Carbohydrate Transport in Bacteria* (Academic, New York).
4. Reizer, J., Saier, M. H., Jr., Deutscher, J., Grenier, F., Thompson, J. & Hengstenberg, W. (1988) *CRC Crit. Rev. Microbiol.* **15**, 297–338.
5. Meadow, N. D., Fox, D. K. & Roseman, S. (1990) *Annu. Rev. Biochem.* **59**, 497–542.
6. Saier, M. H., Jr., & Reizer, J. (1991) *J. Bacteriol.*, in press.
7. Kalbitzer, H. R., Hengstenberg, W., Rosch, P., Muss, P., Bernsmann, P., Engelmann, R., Dörschug, M. & Deutscher, J. (1982) *Biochemistry* **21**, 2879–2885.
8. Reizer, J., Sutrina, S. L., Wu, L.-F., Deutscher, J., Reddy, P. & Saier, M. H., Jr. (1992) *J. Biol. Chem.*, in press.
9. Reizer, J. (1989) *FEMS Microbiol. Rev.* **63**, 149–156.
10. Klevit, R. E. & Waygood, E. B. (1986) *Biochemistry* **25**, 7774–7781.
11. El-Kabbani, O. A. L., Waygood, E. B. & Delbaere, L. T. J. (1987) *J. Biol. Chem.* **262**, 12926–12929.
12. Sharma, S., Georges, F., Delbaere, L. T. J., Lee, J. S., Klevit, R. E. & Waygood, E. B. (1991) *Proc. Natl. Acad. Sci. USA* **88**, 4877–4881.
13. Wittekind, M., Reizer, J., Deutscher, J., Saier, M. H. & Klevit, R. E. (1989) *Biochemistry* **28**, 9908–9912.
14. Wittekind, M., Reizer, J. & Klevit, R. E. (1990) *Biochemistry* **29**, 7191–7200.
15. Reizer, J., Sutrina, S. L., Saier, M. H., Jr., Stewart, G. C., Peterkofsky, A. & Reddy, P. (1989) *EMBO J.* **8**, 2111–2120.
16. Kapadia, G., Reizer, J., Sutrina, S. L., Saier, M. H., Jr., Reddy, P. & Herzberg, O. (1990) *J. Mol. Biol.* **211**, 1–2.
17. Hengstenberg, W. & Deutscher, J. (1987) in *Sugar Transported Metabolism in Gram-Positive Bacteria*, eds. Reizer, J. & Peterkofsky, A. (Horwood, Chichester, England), pp. 215–234.
18. Howard, A. J., Gilliland, G. L., Finzel, B. C., Poulos, T., Ohlendorf, D. O. & Salemme, F. R. (1987) *J. Appl. Crystallogr.* **20**, 383–387.
19. Blundell, T. L. & Johnson, L. N. (1976) *Protein Crystallography* (Academic, London).
20. Dickerson, R. E., Weinzierl, J. E. & Palmer, R. A. (1968) *Acta Crystallogr. Sect. B* **24**, 997–1003.
21. Blow, D. M. & Crick, F. H. C. (1959) *Acta Crystallogr.* **12**, 794–802.
22. Wang, B. C. (1985) *Methods Enzymol.* **115**, 90–112.
23. Jones, T. A. (1982) in *Computational Crystallography*, ed. Sayre, D. (Oxford Univ. Press, London), pp. 303–317.
24. Brünger, A. T., Kuriyan, J. & Karplus, M. (1987) *Science* **235**, 458–460.
25. Hendrickson, W. A. & Konnert, J. H. (1980) in *Biomolecular Structure, Function, Conformation and Evolution*, ed. Srinivasan, R. (Pergamon, Oxford), Vol. 1, pp. 43–75.
26. Finzel, B. C. (1987) *J. Appl. Crystallogr.* **20**, 53–55.
27. Richardson, J. (1981) *Adv. Protein Chem.* **34**, 167–339.
28. Priestle, J. P. (1988) *J. Appl. Crystallogr.* **21**, 572–576.
29. Kabsch, W. & Sander, C. (1983) *Biopolymers* **22**, 2577–2637.
30. Richardson, J. S. & Richardson, D. C. (1988) *Science* **240**, 1648–1652.
31. Kendrew, J. C., Watson, H. C., Stranberg, B. E., Dickerson, E., Phillips, D. C. & Shore, V. C. (1961) *Nature (London)* **190**, 666–670.
32. Liao, D.-I., Kapadia, G., Reddy, P., Saier, M. H., Jr., Reizer, J. & Herzberg, O. (1991) *Biochemistry* **30**, 9583–9594.
33. Begley, G. S., Hansen, D. E., Jacobson, G. R. & Knowles, J. R. (1982) *Biochemistry* **21**, 5552–5556.
34. Knowles, J. R. (1980) *Annu. Rev. Biochem.* **49**, 877–919.